

# A Practical Spectrum Sharing Scheme for Cognitive Radio Networks: Design and Experiments

Pedram Kheirkhah Sangdeh, Hossein Pirayesh, Adnan Quadri, and Huacheng Zeng

**Abstract**—Spectrum shortage is a fundamental problem in wireless networks, and this problem becomes increasingly acute with the rapid proliferation of wireless devices. To address this issue, spectrum sharing in the context of cognitive radio networks (CRNs) has been regarded as a promising solution. Although there is a large body of work on spectrum sharing in the literature, most existing work is limited to theoretical exploration and the progress in practical solution design remains scarce. In this paper, we propose a practical scheme to enable transparent spectrum sharing for a small CRN by leveraging recent advances in multiple-input multiple-output (MIMO) technology. The key components of our scheme are two MIMO-based interference management techniques: blind beamforming (BBF) and blind interference cancellation (BIC). These two techniques enable secondary users to mitigate cross-network interference in the absence of inter-network coordination, fine-grained synchronization, and mutual knowledge. We have built a prototype of our scheme on a wireless testbed and demonstrated its compatibility with commercial Wi-Fi devices (primary users). Experimental results show that, for a secondary device with two/three antennas, BBF and BIC achieve an average of 25 dB and 33 dB interference cancellation capability in real-world wireless environments, respectively.

**Index Terms**—Spectrum sharing, cognitive radio networks, underlay, blind interference cancellation, blind beamforming

## I. INTRODUCTION

The rapid proliferation of wireless devices and the burgeoning demands for wireless services have pushed the spectrum shortage issue to a breaking point. Although it is expected that much spectrum in the millimeter band (30 GHz to 300 GHz) will be allocated for communication purposes, most of this spectrum might be limited to short-range communications due to its severe path loss. Moreover, millimeter band is highly vulnerable to blockage and thus mainly considered for complementary use in next-generation wireless systems. As envisioned, sub-6 GHz frequency spectrum, which is already very crowded, will still be the main carrier for the data traffic in commercial wireless systems. Therefore, it is very necessary to maximize the utilization efficiency of sub-6 GHz spectrum.

To improve spectrum utilization efficiency, spectrum sharing in the context of cognitive radio networks (CRNs) has been widely regarded as a promising and cost-effective solution. In the past two decades, CRNs have received a large amount of research efforts and produced many cognitive radio schemes. Depending on the spectrum access strategy at secondary users, the existing cognitive radio schemes can be classified to

The authors are with the Department of Electrical and Computer Engineering, University of Louisville, Louisville, KY 40292.

This work is supported in part by NSF grants CNS-1717840 and CNS1846105.

Part of this work was presented in IEEE Infocom 2019 [1].

three paradigms: interweave, overlay, and underlay [2]. In the *interweave* paradigm, secondary users exploit spectrum white holes and intend to access the spectrum opportunistically when primary users are idle. In the *overlay* paradigm, secondary users are allowed to access spectrum simultaneously with primary users, provided that the primary users share the knowledge of their signal codebooks and messages with the secondary users. Compared to these two paradigms, the *underlay* paradigm is more appealing as it allows secondary users to concurrently utilize the spectrum with primary users while requiring neither coordination nor knowledge from the primary users.

Although there is a large body of work on underlay CRNs in the literature, most of existing work is either focused on theoretical exploration or reliant on unrealistic assumptions such as cross-network channel knowledge and inter-network coordination (see, e.g., [3]–[11]). Thus far, very limited progress has been made in the design of practical underlay spectrum sharing schemes. To the best of our knowledge, there is no underlay spectrum sharing scheme that has been implemented and validated in real-world wireless environments. This stagnation underscores the challenge in such a design, which is reflected in the following two tasks: i) at a secondary transmitter, how to pre-cancel its generated interference for the primary receivers in its close proximity; and ii) at a secondary receiver, how to decode its desired signals in the presence of unknown interference from primary transmitters. These two tasks become even more challenging when secondary users have no knowledge (e.g., signal waveform and frame structure) about primary users.

In this paper, we consider an underlay CRN that comprises a pair of primary users and a pair of secondary users. We assume that the secondary users are equipped with more antennas than the primary users. By leveraging their multiple antennas, the secondary users take the full responsibility for cross-network interference cancellation (IC). For such a CRN, we propose a practical spectrum sharing scheme that allows the secondary users to access the spectrum while remaining transparent to the primary users. The key components of our scheme are two interference management techniques: blind beamforming (BBF) and blind interference cancellation (BIC).

The proposed BBF technique is used at the secondary transmitter to pre-cancel its generated interference for the primary receiver. In contrast to existing beamforming techniques, which require channel knowledge for the construction of beamforming filters, our BBF technique does not require channel knowledge. Instead, it constructs the beamforming filters by exploiting the statistical characteristics of the overheard interfering signals from the primary users. The proposed

BIC technique is used at the secondary receiver to decode its desired signals in the presence of unknown interference from the primary transmitter. Unlike existing IC techniques, which require channel state information (CSI) and inter-network synchronization, our BIC technique requires neither cross-network channel knowledge nor inter-network synchronization for signal detection. Rather, it leverages the reference symbols (preamble) embedded in the data frame of secondary users to construct the decoding filters for signal detection in the face of unknown interference. With these two IC techniques, the secondary users can effectively mitigate the cross-network interference in the absence of coordination from the primary users.

We have built a prototype of our scheme on a wireless testbed to evaluate its performance in real-world wireless environments. Particularly, we have demonstrated that our prototyped secondary devices can share 2.4 GHz spectrum with commercial Wi-Fi devices (primary users) while not affecting Wi-Fi devices' throughput. A demo video of our scheme is presented in [12]. We further conduct experiments to evaluate the performance of our secondary network in coexistence with LTE-like and CDMA-like primary networks in the following two cases: i) the primary users are equipped with one antenna and the secondary users equipped with two antennas; and ii) the primary users are equipped with two antennas and the secondary users equipped with three antennas. Experimental results measured in an office environment show that the secondary network can achieve an average of 1.1 bits/s/Hz spectrum utilization without visibly degrading primary network throughput. Moreover, the proposed BBF and BIC techniques achieve an average of 25 dB and 33 dB IC capabilities, respectively.

The contributions of this paper are summarized as follows:

- We have designed a new BIC technique for a wireless receiver, which is capable of decoding its data packets in the presence of unknown interference. Our prototype of such a wireless receiver can achieve 33 dB IC capability for unknown interference in real-world tests.
- We have designed a new BBF technique for a wireless transmitter, which is capable of pre-canceling its generated interference for an unintended receiver without the need of channel knowledge. Our prototype of such a wireless transmitter can achieve 25 dB IC capability for the unintended receiver.
- To the best of our knowledge, our work is the first one that demonstrates real-time concurrent spectrum utilization of two wireless systems in the absence of inter-network coordination and fine-grained synchronization.

The remainder of this paper is organized as follows. Section II surveys the related work. Section III clarifies the problem and system model. Section IV offers an overview of the proposed spectrum sharing scheme at the MAC and PHY layers. Section V and Section VI present the proposed BBF and BIC techniques, respectively. Section VII presents our experimental results. Section VIII discusses the limitations of our scheme, and Section IX concludes this paper.

## II. RELATED WORK

We focus our literature survey on spectrum sharing in underlay CRNs and the related interference management techniques.

**Spectrum Sharing in Underlay CRNs:** Underlay CRNs allow concurrent spectrum utilization for primary and secondary networks as long as the interference at primary users remains at an acceptable level. Different signal processing techniques have been studied for interference management in underlay CRNs, such as spread spectrum [13], power control [6]–[8], and beamforming [14]–[32]. Spread spectrum handles interference in the code domain, and power control tames interference in the power domain. Beamforming exploits the spatial degrees of freedom (DoF) provided by multiple antennas to steer the secondary signals to some particular directions, thereby avoiding interference for primary users. Compared to the other two techniques, beamforming is more appealing in practice as it is effective in interference management.

Given its potential, beamforming has been studied in underlay CRNs to pursue various objectives, such as improving energy efficiency of secondary transmissions [14]–[17], maximizing data rate of secondary users [22], [23], maximizing sum rate of both primary and secondary users [18]–[21], and enhancing the security against eavesdroppers [24]–[26]. However, most of these beamforming solutions are reliant on global network information and cross-network channel knowledge. Our work differs from these efforts as it requires neither cross-network channel knowledge nor inter-network cooperation.

**BBF in Underlay CRNs:** There are some pioneering works that studied BBF to eliminate the requirement of cross-network channel knowledge for the design of beamforming filters [27]–[32]. In [27] and [28], an eigen-value-decomposition-based approach was proposed to construct beamforming filters at a secondary transmitter using its received interfering signals from a primary device. When the secondary device transmitting, the constructed beamforming filters would steer its radio signals to the null subspace of the cross-network channel, thereby avoiding interference for the primary device. Our BBF technique follows similar idea, but differs in the network setting and design objective. Specifically, [27] and [28] were focused on theoretical analysis to optimize the data rate of secondary users under certain interference temperature, while the BBF technique in our work is designed to guarantee its practicality and optimize its IC capability in real-world OFDM-based networks.

In [29] and [30], the beamforming design is formulated as a part of a network optimization problem, and some constraints are developed based on statistical channel knowledge to relax the requirement of cross-network channel knowledge. This approach is of high complexity, and it seems not amenable to practical implementation. In [31] and [32], spatial learning methods were proposed to iteratively adjust beamforming filters at the secondary devices based on the power level of primary transmission, with the objective of reducing cross-network interference for primary users. However, these learning-based methods are cumbersome and not amenable to practical use.

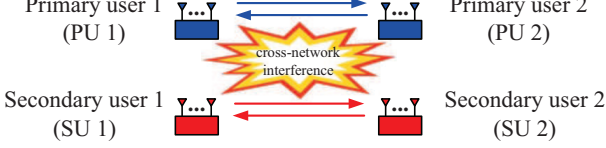


Fig. 1: A CRN consisting of two active primary users and two active secondary users.

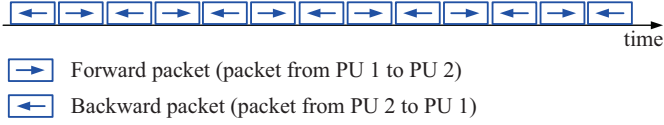


Fig. 2: Consistent and persistent traffic in the primary network.

**MIMO-based BIC:** While there are many results on interference cancellation in cooperative wireless networks, the results of MIMO-based BIC in non-cooperative networks remain limited. In [33], Rousseaux et al. proposed a MIMO-based BIC technique to handle interference from one source. In [34], Winters proposed a spatial filter design for signal detection at multi-antenna wireless receivers to combat unknown interference. In [35], Gollakota et al. proposed a MIMO-based solution to mitigate narrow-band interference from home devices such as microwave. BIC was further studied in the context of radio jamming in wireless communications (see, e.g., [36], [37]). Compared to the existing BIC techniques, our BIC technique has a lower complexity and offers much better performance (33 dB IC capability in our experiments).

### III. PROBLEM STATEMENT

We consider an underlay CRN as shown in Fig. 1, which consists of two active primary users and two secondary users. The primary users establish bidirectional communications in time-division duplex (TDD) mode. The traffic flow in the primary network is persistent and consistent in both directions, as shown in Fig. 2. The secondary users want to utilize the same spectrum for their own communications. To do so, the secondary transmitter employs beamforming to pre-cancel its generated interference for the primary receiver; and the secondary receiver performs IC for its signal detection. Simply put, the secondary users take full burden of cross-network interference cancellation, and their data transmissions are transparent to the primary users.

In this CRN, there is no coordination between the primary and secondary users. The secondary users have no knowledge about cross-network interference characteristics. The primary users have one or multiple antennas, and the number of their antennas is denoted by  $M_p$ . The secondary users have multiple antennas, and the number of their antennas is denoted by  $M_s$ . We assume that the number of antennas on a secondary user is greater than that on a primary user, i.e.,  $M_s > M_p$ . This assumption ensures that each secondary user has sufficient spatial DoF to tame cross-network interference.

**Our Objective:** In such a CRN, our objective is four-fold: i) design a BBF technique for the secondary transmitter to pre-cancel its generated interference for the primary receiver; ii) design a BIC technique for the secondary receiver to decode

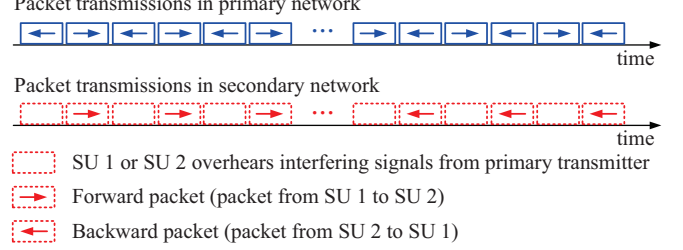


Fig. 3: A MAC protocol for spectrum sharing in a CRN that has two primary users and two secondary users.

its desired signals in the presence of interference from the primary transmitter; iii) design a spectrum sharing scheme by integrating these two IC techniques; and iv) evaluate the IC techniques and the spectrum sharing scheme via experimentation in real wireless environments.

**Two Justifications:** First, in this paper, we study a CRN that comprises one pair of primary users and one pair of secondary users. Although it has a small network size, such a CRN serves as a fundamental building block for a large-scale CRN that have many primary and secondary users. Therefore, understanding this small CRN is of both theoretical and practical importance. Second, in our study, we assume that the secondary users have no knowledge about cross-network interference characteristics. Such a conservative assumption leads to a more robust spectrum sharing solution, which is suited for many application scenarios.

### IV. A SPECTRUM SHARING SCHEME

In this section, we present a spectrum sharing scheme for the secondary network so that it can use the same spectrum for its communications while almost not affecting performance of the primary network. Our scheme consists of a lightweight MAC protocol and a new PHY design for the secondary users. In what follows, we first present the MAC protocol and then describe the new PHY design.

#### A. MAC Protocol for Secondary Network

Fig. 3 shows our MAC protocol in the time domain. It includes both forward communications (from SU 1 to SU 2) and backward communications (from SU 2 to SU 1) between the two secondary users. Since the two communications are symmetric, our presentation in the following will focus on the forward communications. The backward communications can be done in the same way.

The forward communications in the proposed MAC protocol comprise two phases: *overhearing (Phase I)* and *packet transmission (Phase II)*. In the time domain, Phase I aligns with the backward packet transmissions of the primary network, and Phase II aligns with the forward packet transmissions of the primary network, as illustrated in Fig. 3. We elaborate the operations in the two phases as follows:

- **Phase I:** SU 1 overhears the interfering signals from PU 2, and SU 2 remains idle, as shown in Fig. 4(a).

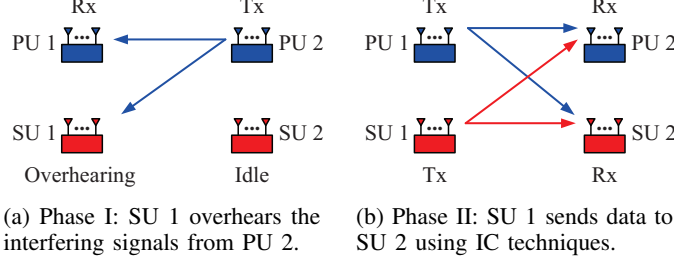


Fig. 4: Illustration of our proposed spectrum sharing scheme.

- **Phase II:** SU 1 first constructs beamforming filters using the overheard interfering signals in Phase I and then transmits signals to SU 2 using the constructed beamforming filters. Meanwhile, SU 2 decodes the signals from SU 1 in the presence of interference from PU 1. Fig. 4(b) shows the packet transmission in this phase.

When the primary network has consistent and persistent bidirectional traffic, it is easy for secondary devices to learn primary transmission direction and duration by leveraging wireless signals' spatial signature (e.g., signal angle-of-arrival). Based on the learned information, the secondary network can align its transmissions with the transmissions in the primary network, as illustrated in Fig. 3. It is noteworthy that the time alignment requirement of primary and secondary transmissions is loose, thanks to the capability of BBF and BIC at the PHY layer. To ensure that the secondary transmissions will not disrupt the primary transmissions, SU 1 sends its signals only after it detects the interfering signals from PU 2.

### B. PHY Design for Secondary Users: An Overview

To support the proposed MAC protocol, we use the IEEE 802.11 legacy PHY for the secondary network, including the frame structure, OFDM modulation, and channel coding schemes. However, IEEE 802.11 legacy PHY is vulnerable to cross-network interference. Therefore, we need to modify the legacy PHY for the secondary users. The modified PHY should be resilient to cross-network interference on both transmitter and receiver sides. The design of such a PHY faces the following two challenges.

**Challenge 1:** Referring to Fig. 4(b), the main task of the secondary transmitter (SU 1) is to pre-cancel its generated interference for the primary receiver (PU 2). Note that we assume the secondary transmitter has no knowledge about the primary network, including the signal waveform, bandwidth, and frame structure. The primary network may use OFDM, CDMA, or other types of modulation for packet transmission. The lack of knowledge about the interference makes it challenging for SU 1 to cancel the interference.

To address this challenge, we design a BBF technique for the secondary transmitter (SU 1) to pre-cancel its interference at the primary receiver. Our beamforming technique takes advantage of the overheard interfering signals in Phase I to construct precoding vectors for beamforming. Our BBF technique can completely pre-cancel the interference at the primary receiver if noise is zero and the reciprocity of for-

ward/backward channels is maintained. Details of this beamforming technique are presented in Section V.

**Challenge 2:** Referring to Fig. 4(b) again, the main task of the secondary receiver (SU 2) is to decode its desired signals in the presence of unknown cross-network interference. Note that the secondary receiver has no knowledge about the interference characteristics, and the primary and secondary networks may use different waveforms and frame formats for their transmissions. The lack of inter-network coordination, cross-network knowledge and fine-grained synchronization makes it challenging to tame interference for signal detection.

To address this challenge, we design a MIMO-based BIC technique for the secondary receiver. The core component of our BIC technique is a spatial filter, which mitigates unknown cross-network interference from the primary transmitter and recovers the desired signals. Details of this BIC technique are presented in Section VI.

### V. BLIND BEAMFORMING

In this section, we study the beamforming technique at SU 1 in Fig. 4. In Phase I, SU 1 first overhears the interfering signals from the primary transmitter and then uses the overheard interfering signals to construct spatial filters. Based on channel reciprocity, the constructed spatial filters are used as beamforming filters in Phase II to avoid interference at the primary receiver. These operations are performed on each subcarrier in the OFDM modulation. In what follows, we first present the derivation of beamforming filters and then offer performance analysis of the proposed beamforming technique.

**Mathematical Formulation:** Consider SU 1 in Fig. 4(a). It overhears interfering signals from PU 2. The overheard interfering signals are converted to the frequency domain through FFT operation.<sup>1</sup> We assume that the channel from PU 2 to SU 1 is a block-fading channel in the time domain. That is, all the OFDM symbols in the backward transmissions experience the same channel. Denote  $\mathbf{Y}(l, k)$  as the  $l$ th sample of the overheard interfering signal on subcarrier  $k$  in Phase I. Then, we have<sup>2</sup>

$$\mathbf{Y}(l, k) = \mathbf{H}_{\text{sp}}^{[1]}(k)\mathbf{X}_p^{[1]}(l, k) + \mathbf{W}(l, k), \quad (1)$$

where  $\mathbf{H}_{\text{sp}}^{[1]}(k) \in \mathbb{C}^{M_s \times M_p}$  is the matrix representation of the block-fading channel from PU 2 to SU 1 on subcarrier  $k$ ,  $\mathbf{X}_p^{[1]}(l, k) \in \mathbb{C}^{M_p \times 1}$  is the interfering signal transmitted by PU 2 on subcarrier  $k$ , and  $\mathbf{W}(l, k) \in \mathbb{C}^{M_s \times 1}$  is the noise vector at SU 1. It is noteworthy that SU 1 knows  $\mathbf{Y}(l, k)$  but does not know  $\mathbf{H}_{\text{sp}}^{[1]}(k)$ ,  $\mathbf{X}_p^{[1]}(l, k)$ , and  $\mathbf{W}(l, k)$ .

At SU 1, we seek a spatial filter that can combine the overheard interfering signals in a destructive manner. Denote  $\mathbf{P}(k)$  as the spatial filter on subcarrier  $k$ . Then, the problem of designing  $\mathbf{P}(k)$  can be expressed as:

$$\min \mathbb{E}[\mathbf{P}(k)^*\mathbf{Y}(l, k)\mathbf{Y}(l, k)^*\mathbf{P}(k)], \quad \text{s.t. } \mathbf{P}(k)^*\mathbf{P}(k) = 1, \quad (2)$$

<sup>1</sup>The interfering signals are not necessarily OFDM signals.

<sup>2</sup>For the notation in this paper, superscripts "[1]" and "[2]" mean Phase I and Phase II, respectively. Subscripts "s" and "p" mean the secondary and primary users, respectively.

where  $(\cdot)^*$  represents conjugate transpose operator.

**Construction of Spatial Filters:** To solve the optimization problem in (2), we use Lagrange multipliers method. We define the Lagrange function as:

$$\mathcal{L}(\mathbf{P}(k), \lambda) = \mathbb{E}[\mathbf{P}(k)^* \mathbf{Y}(l, k) \mathbf{Y}(l, k)^* \mathbf{P}(k)] - \lambda [\mathbf{P}(k)^* \mathbf{P}(k) - 1], \quad (3)$$

where  $\lambda$  is Lagrange multiplier.

By setting the partial derivatives of  $\mathcal{L}(\mathbf{P}(k), \lambda)$  to zero, we have

$$\frac{\partial \mathcal{L}(\mathbf{P}(k), \lambda)}{\partial \mathbf{P}(k)} = \mathbf{P}(k)^* (\mathbb{E}[\mathbf{Y}(l, k) \mathbf{Y}(l, k)^*] - \lambda \mathbf{I}) = 0, \quad (4)$$

$$\frac{\partial \mathcal{L}(\mathbf{P}(k), \lambda)}{\partial \lambda} = \mathbf{P}(k)^* \mathbf{P}(k) - 1 = 0. \quad (5)$$

Based on the definition of eigendecomposition, it is easy to see that the solutions to equations (4) and (5) are the eigenvectors of  $\mathbb{E}[\mathbf{Y}(l, k) \mathbf{Y}(l, k)^*]$  and the corresponding values of  $\lambda$  are the eigenvalues of  $\mathbb{E}[\mathbf{Y}(l, k) \mathbf{Y}(l, k)^*]$ . Note that  $\mathbb{E}[\mathbf{Y}(l, k) \mathbf{Y}(l, k)^*]$  has  $M_s$  eigenvectors, each of which corresponds to a stationary point of the Lagrange function (extrema, local optima, and global optima). As  $\lambda$  is the penalty multiplier for the Lagrange function, the optimal spatial filter  $\mathbf{P}(k)$  lies within the subspace spanned by the eigenvectors of  $\mathbb{E}[\mathbf{Y}(l, k) \mathbf{Y}(l, k)^*]$  that correspond to the minimum eigenvalue.

For Hermitian matrix  $\mathbb{E}[\mathbf{Y}(l, k) \mathbf{Y}(l, k)^*]$ , it may have multiple eigenvectors that correspond to the minimum eigenvalue. Denote  $M_e$  as the number of eigenvectors that correspond to the minimum eigenvalue. Then, we can write them as:

$$[\mathbf{U}_1, \mathbf{U}_2, \dots, \mathbf{U}_{M_e}] = \text{mineigvectors}\left(\mathbb{E}[\mathbf{Y}(l, k) \mathbf{Y}(l, k)^*]\right), \quad (6)$$

where  $\text{mineigvectors}(\cdot)$  represents the eigenvectors that correspond to the minimum eigenvalue.

To estimate  $\mathbb{E}[\mathbf{Y}(l, k) \mathbf{Y}(l, k)^*]$  in (6), we average the received interfering signal samples over time. Denote  $\mathbf{Y}(l, k)$  as the  $l$ th sample of the received interfering signals on subcarrier  $k$ . Then, we have

$$[\mathbf{U}_1, \mathbf{U}_2, \dots, \mathbf{U}_{M_e}] = \text{mineigvectors}\left(\sum_{l=1}^{L_p} \mathbf{Y}(l, k) \mathbf{Y}(l, k)^*\right), \quad (7)$$

where  $L_p$  is the number of overheard interfering signal samples (e.g.,  $L_p = 20$ ). Also, the neighboring subcarriers can be bonded to improve accuracy. Based on (7), the optimal filter  $\mathbf{P}(k)$  can be written as:

$$\mathbf{P}(k) = \sum_{m=1}^{M_e} \alpha_m \mathbf{U}_m, \quad (8)$$

where  $\alpha_m$  is a weight coefficient with  $\sum_{m=1}^{M_e} \alpha_m^2 = 1$ .

Now, we summarize the BBF technique as follows. In Phase I, SU 1 overhears the interfering signal  $\mathbf{Y}(l, k)$  from PU 2. Based on the overheard interfering signals, it constructs a spatial filter  $\mathbf{P}(k)$  for subcarrier  $k$  using (7) and (8). In Phase II, we use  $\overline{\mathbf{P}(k)}$  as the precoding vector for beamforming on subcarrier  $k$ , where  $(\cdot)$  is the element-wise conjugate operator.

For this beamforming technique, we have the following remarks: i) This beamforming technique does not require CSI. Rather, it uses the overheard interfering signals to construct the precoding vectors for beamforming. ii) This beamforming technique requires only one-time eigendecomposition on every subcarrier. It has a computational complexity similar to zero-forcing (ZF) and minimum mean square error (MMSE) precoding techniques. Therefore, it is amenable to practical implementation.

**IC Capability of BBF:** For the performance of the proposed beamforming technique, we have the following lemma:

*Lemma 1: The proposed beamforming technique completely pre-cancels interference at the primary receiver if (i) forward and backward channels are reciprocal; and (ii) noise is zero.*

The proof of Lemma 1 is provided in Appendix A. To maintain the reciprocity of forward and backward channels in practical wireless systems, we can employ the relative calibration method in [38]. This relative calibration method is an internal and standalone method that can be done with assistance from one device. In our experiments, we have implemented this calibration method to preserve the channels reciprocity.

## VI. BLIND INTERFERENCE CANCELLATION

In this section, we focus on SU 2 in Phase II as shown in Fig. 4(b). We design a BIC technique for the secondary receiver (SU 2) to decode its desired signals in the presence of interference from the primary transmitter (PU 1).

**Mathematical Formulation:** Recall that we use IEEE 802.11 legacy PHY for data transmissions in the secondary network. Specifically, SU 1 sends packet-based signals to SU 2, which comprise a bulk of OFDM symbols. In each packet, the first four OFDM symbols carry pREAMbles (pre-defined reference signals) and the remaining OFDM symbols carry payloads.

Consider the signal transmission in Fig. 4(b). Denote  $X_s^{[2]}(l, k)$  as the signal that SU 1 transmits on subcarrier  $k$  in OFDM symbol  $l$ . Denote  $\mathbf{X}_p^{[2]}(l, k)$  as the signal that PU 1 transmits on subcarrier  $k$  in OFDM symbol  $l$ .<sup>3</sup> Denote  $\mathbf{Y}(l, k)$  as the received signal vector at SU 2 on subcarrier  $k$  in OFDM symbol  $l$ . Then, we have

$$\mathbf{Y}(l, k) = \mathbf{H}_{ss}^{[2]}(k) \overline{\mathbf{P}(k)} X_s^{[2]}(l, k) + \mathbf{H}_{sp}^{[2]}(k) \mathbf{X}_p^{[2]}(l, k) + \mathbf{W}(l, k), \quad (9)$$

where  $\mathbf{H}_{ss}^{[2]}(k)$  is the block-fading channel between SU 2 and SU 1 on subcarrier  $k$ ,  $\mathbf{H}_{sp}^{[2]}(k)$  is the block-fading channel between SU 2 and PU 1 on subcarrier  $k$ , and  $\mathbf{W}(l, k)$  is noise on subcarrier  $k$  in OFDM symbol  $l$ .

At SU 2, in order to decode the intended signal in the presence of cross-network interference, we use a linear spatial filter  $\mathbf{G}(k)$  for all OFDM symbols on subcarrier  $k$ . Then, the decoded signal can be written as:

$$\hat{\mathbf{X}}_s^{[2]}(l, k) = \mathbf{G}(k)^* \mathbf{Y}(l, k). \quad (10)$$

While there exist many criteria for the design of  $\mathbf{G}(k)$ , our objective is to minimize the mean square error (MSE) between

<sup>3</sup>PU 1 does not necessarily send OFDM signals. But at SU 2, the interfering signals from PU 1 can always be converted to the frequency domain using FFT operation.

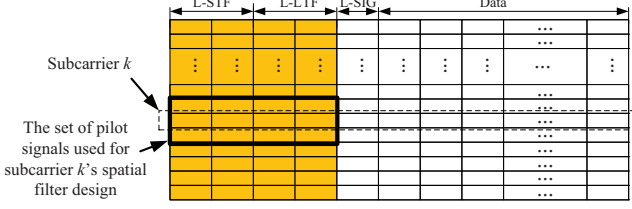


Fig. 5: An example of  $\mathcal{Q}(k)$  in IEEE 802.11 legacy frame.

the decoded and original signals. Thus, the signal detection problem can be formulated as:

$$\min \mathbb{E} \left[ \left| \hat{X}_s^{[2]}(l, k) - X_s^{[2]}(l, k) \right|^2 \right]. \quad (11)$$

**Construction of Spatial Filters:** To solve the optimization problem in (11), we use Lagrange multipliers method again. We define the Lagrange function as:

$$\mathcal{L}(\mathbf{G}(k)) = \mathbb{E} \left[ \left| \hat{X}_s^{[2]}(l, k) - X_s^{[2]}(l, k) \right|^2 \right]. \quad (12)$$

Based on (10), (12) can be rewritten as:

$$\mathcal{L}(\mathbf{G}(k)) = \mathbb{E} \left[ \left| \mathbf{G}(k)^* \mathbf{Y}(l, k) - X_s^{[2]}(l, k) \right|^2 \right]. \quad (13)$$

Equation (13) is a quadratic function of  $\mathbf{G}(k)$ . To minimize MSE, we can take the gradient with respect to  $\mathbf{G}(k)$ . The optimal filter  $\mathbf{G}(k)$  can be obtained by setting the gradient to zero, which we show as follows:

$$\mathbb{E}[\mathbf{Y}(l, k)\mathbf{Y}(l, k)^*]\mathbf{G}(k) - \mathbb{E}[\mathbf{Y}(l, k)X_s^{[2]}(l, k)^*] = 0. \quad (14)$$

Based on (14), we obtain the optimal filter

$$\mathbf{G}(k) = \mathbb{E}[\mathbf{Y}(l, k)\mathbf{Y}(l, k)^*]^+ \mathbb{E}[\mathbf{Y}(l, k)X_s^{[2]}(l, k)^*], \quad (15)$$

where  $(\cdot)^+$  denotes pseudo inverse operation. Equation (15) is the optimal design of  $\mathbf{G}(k)$  in the sense of minimizing MSE. To calculate  $\mathbb{E}[\mathbf{Y}(l, k)\mathbf{Y}(l, k)^*]$  and  $\mathbb{E}[\mathbf{Y}(l, k)X_p^{[2]}(l, k)^*]$  in (15), we can take advantage of the pilot (reference) symbols in wireless systems (e.g., the preamble in IEEE 802.11 legacy frame). Denote  $\mathcal{Q}_k$  as the set of pilot symbols in a frame that can be used for the design of interference mitigation filter  $\mathbf{G}(k)$ . Then, we can approach the statistical expectations in (15) using the averaging operations as follows:

$$\mathbb{E}[\mathbf{Y}(l, k)\mathbf{Y}(l, k)^*] \approx \frac{1}{|\mathcal{Q}_k|} \sum_{(l, k') \in \mathcal{Q}_k} \mathbf{Y}(l, k')\mathbf{Y}(l, k')^*, \quad (16)$$

$$\mathbb{E}[\mathbf{Y}(l, k)X_p^{[2]}(l, k)^*] \approx \frac{1}{|\mathcal{Q}_k|} \sum_{(l, k') \in \mathcal{Q}_k} \mathbf{Y}(l, k')X_p^{[2]}(l, k')^*, \quad (17)$$

where an example of  $\mathcal{Q}_k$  is illustrated in Fig. 5.

Note that, with a bit abuse of notation, we replace the approximation sign in (16) and (17) with an equation sign for simplicity. Then, the spatial filter  $\mathbf{G}(k)$  can be written as:

$$\mathbf{G}(k) = \left[ \sum_{(l, k') \in \mathcal{Q}_k} \mathbf{Y}(l, k')\mathbf{Y}(l, k')^* \right]^+ \left[ \sum_{(l, k') \in \mathcal{Q}_k} \mathbf{Y}(l, k')X_p^{[2]}(l, k')^* \right]. \quad (18)$$

We now summarize our BIC technique as follows. In

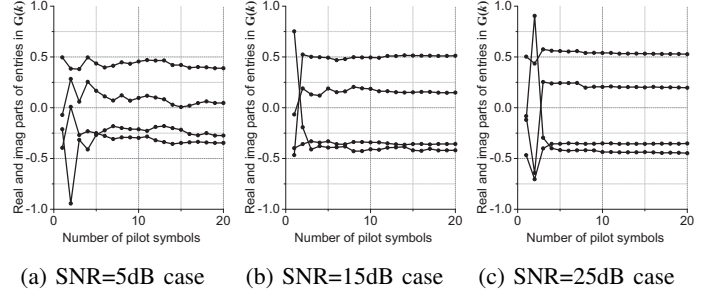


Fig. 6: Convergence speed of spatial filter over the number of pilot symbols in ( $M_p = 1, M_s = 2$ ) network.

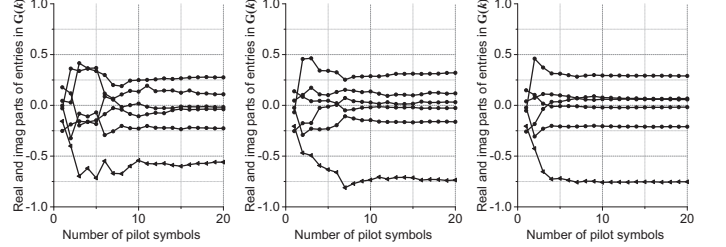


Fig. 7: Convergence speed of spatial filter over the number of pilot symbols in ( $M_p = 2, M_s = 3$ ) network.

Phase II, SU 2 needs to decode its desired signal in the presence of interference from PU 1. To do so, SU 2 first constructs a spatial filter for each of its subcarriers using (18), and then decodes its desired signal using (10).

For this BIC technique, several remarks are in order: i) The spatial filter in (18) not only cancels the interference but also equalizes the channel distortion for signal detection. ii) As shown in (10) and (18), our BIC technique does not require knowledge about the interference characteristics, including waveform and bandwidth. iii) our BIC technique does not require CSI. Rather, it only requires pilot signals at the secondary transmitter. In contrast to conventional signal detection techniques (e.g., ZF and MMSE detectors), our BIC technique does not require channel estimation. iv) As shown in (10) and (18), the computational complexity of our BIC technique is similar to that of the ZF detector, which is widely being used in real-world wireless systems.

**IC Capability of BIC:** For the performance of the proposed BIC technique, we have the following lemma:

**Lemma 2:** If the pilot signals are sufficient and noise is zero, the BIC technique can perfectly recover the desired signals in the presence of cross-network interference (i.e.,  $\hat{X}_s^{[2]}(k, l) = X_s^{[2]}(k, l), \forall k, l$ ).

The proof of Lemma 2 is presented in Appendix B.

**Pilot Signals for Spatial Filter Construction:** Lemma 2 shows the superior performance of our BIC technique when the pilot signals are sufficient. A natural question to ask is how many pilot signals are considered to be sufficient. To answer this question, we first present our simulation results to study the convergence speed of the spatial filter over the number of pilot signals, and then propose a method to increase the number of pilot signals for the spatial filter construction.

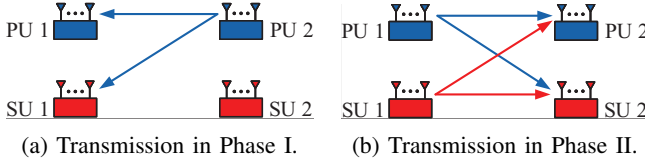


Fig. 8: Experimental setup for an underlay CRN with two network settings: ( $M_p=1, M_s=2$ ) and ( $M_p=2, M_s=3$ ).

As an instance, we simulated the convergence speed of the spatial filter over the number of pilot symbols for SU 2 in Fig. 4. Fig. 6 and Fig. 7 present our simulation results in two network settings: ( $M_p = 1, M_s = 2$ ) and ( $M_p = 2, M_s = 3$ ). From the simulation results, we can see that the spatial filter converges at a pretty fast speed in these two network settings. Specifically, the spatial filter can achieve a good convergence within about 10 pilot symbols.

Recall that the secondary network uses IEEE 802.11 legacy frame for transmissions from SU 1 to SU 2, which only has four pilot symbols on each subcarrier (i.e., two L-STF OFDM symbols and two L-LTF OFDM symbols). So, the construction of spatial filter is in shortage of pilot symbols. To address this issue, for each subcarrier, we not only use the pilot symbols on that subcarrier but also the pilot symbols on its neighboring subcarriers, as illustrated in Fig. 5. The rationale behind this operation lies in the fact that channel coefficients on neighboring subcarriers are highly correlated in real-world wireless environments. By leveraging the pilot symbols on two neighboring subcarriers, we have 12 pilot symbols for the construction of the spatial filter, which appears to be sufficient based on our simulation results in Fig. 6 and Fig. 7. We note that analytically studying the performance of BIC with respect to the number and format of pilot signals is beyond the scope of this work. Instead, we resort to experiments to study its performance in real-world network settings.

## VII. PERFORMANCE EVALUATION

In this section, we consider an underlay CRN in two time slots as shown in Fig. 8. We have built a prototype of the proposed underlay spectrum sharing scheme in this network on a software-defined radio (SDR) testbed and evaluated its performance in real-world wireless environments.

### A. Implementation

**PHY Implementation:** We consider three different primary networks: a commercial Wi-Fi primary network, a LTE-like primary network, and a CDMA-like primary network. The commercial Wi-Fi network comprises Alfa AWUS036NHA 802.11n Adapters, each of which has one antenna for radio signal transmissions and receptions. The LTE-like and CDMA-like primary networks as well as the secondary network are built using USRP N210 devices and general-purpose computers. The USRP devices are used for radio signal transmission/reception while the computers are used for baseband signal processing and MAC protocol implementation. The implementation parameters are listed in Table I.

TABLE I: The implementation parameters of primary and secondary networks.

	Primary network 1	Primary network 2	Primary network 3	Secondary network
System type	Commercial	Custom-built	Custom-built	Custom-built
Standard	Wi-Fi	LTE-like	CDMA-like	Wi-Fi-like
Waveform	OFDM	OFDM	CDMA	OFDM
FFT-Point	64	1024	-	64
Valid subcarriers	52	600	-	52
Sample rate	20 MSps	10 MSps	5 MSps	5, 25 MSps
Signal bandwidth	~16 MHz	~5.8 MHz	~5 MHz	~4.06, 20.31 MHz
Carrier frequency	2.48 GHz	2.48 GHz	2.48 GHz	2.48 GHz
Max tx power	~20 dBm	~15 dBm	~15 dBm	~15 dBm
Antenna number	1	1, 2	1	2, 3

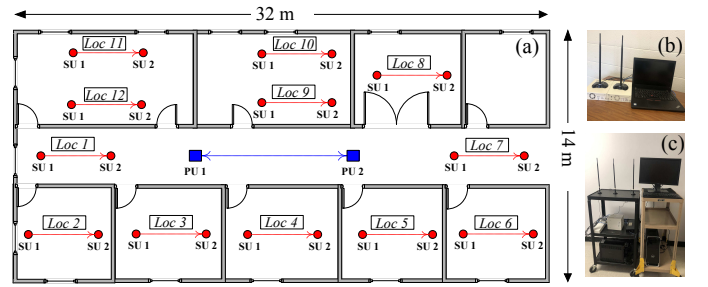


Fig. 9: Experimental setting: (a) floor plan of primary and secondary users' locations; (b) a primary transceiver; and (c) a secondary transceiver.

**MAC Implementation:** We implement the MAC protocol in Fig. 3 for the primary and secondary networks. The packet transmissions in the two networks are loosely aligned in time, as shown in Fig. 3. Since the bidirectional communications in the secondary network are symmetric, we only consider the forward communications (from SU 1 to SU 2) in our experiments. We implement BBF on SU 1 to pre-cancel interference for the primary receiver. We also implement BIC on SU 2 to decode its desired signals in the presence of interference from PU 1. Moreover, we implement the RF chain calibration method [38] on SU 1 in Fig. 8 to maintain its relative channel reciprocity. Note that the calibration needs to be done at a low frequency (0.1 Hz in our experiments) and therefore would not consume much airtime resource.

### B. Experimental Setup and Performance Metrics

**Experimental Setup:** Consider the primary and secondary networks in Fig. 8. We place the devices on a floor plan as shown in Fig. 9(a). The two primary users are always placed at the spots marked “PU 1” and “PU 2.” The two secondary users are placed at one of the 12 different locations. The distance between PU 1 and PU 2 is 10 m and the distance between SU 1 and SU 2 is 6 m. Fig. 9(b-c) show the prototyped secondary and primary transceivers on our wireless testbed. The transmit power of primary users is fixed to the maximum level specified in Table I, while the transmit power of secondary users is properly adjusted to ensure that its generated interference to the primary receiver (after BBF) is below noise level.

**Performance Metrics:** We evaluate the performance of the proposed spectrum sharing scheme using the following four metrics: *i) Tx-side IC capability at SU 1:* This IC capability is from SU 1’s BBF. It is defined as  $\beta_{tx} = 10 \log_{10}(P_1/P_2)$ ,

TABLE II: EVM specification in IEEE 802.11ac standard [39].

EVM (dB)	(inf -5)	[−5 −10]	[−10 −13]	[−13 −16]	[−16 −19]	[−19 −22]	[−22 −25]	[−25 −27]	[−27 −30]	[−30 −32]	[−32 −inf]
Modulation	N/A	BPSK	QPSK	QPSK	16QAM	16QAM	64QAM	64QAM	64QAM	256QAM	256QAM
Coding rate	N/A	1/2	1/2	3/4	1/2	3/4	2/3	3/4	5/6	3/4	5/6
$\gamma$ (EVM)	0	0.5	1	1.5	2	3	4	4.5	5	6	20/3

TABLE III: EVM specification for LTE-like PHY [40], [41].

EVM (dB)	[−6.3 −9.1]	[−9.1 −11.8]	[−11.8 −14.2]	[−14.2 −16.8]	[−16.8 −19.1]
CQI	6	7	8	9	10
Modulation	QPSK	16QAM	16QAM	16QAM	64QAM
Coding rate $\times 1024$	602	378	490	616	466
$\gamma$ (EVM)	1.1758	1.4766	1.9141	2.4063	2.7305
EVM (dB)	[−19.1 −21.0]	[−21.0 −23.3]	[−23.3 −25.7]	[−25.7 −28.2]	[−28.2 −∞)
CQI	11	12	13	14	15
Modulation	64QAM	64QAM	64QAM	64QAM	64QAM
Coding rate $\times 1024$	567	666	772	873	948
$\gamma$ (EVM)	3.3223	3.9023	4.5234	5.1152	5.5547

where  $P_1$  is the received interference power at PU 2 when SU 1 uses  $[\frac{1}{\sqrt{2}} \frac{1}{\sqrt{2}}]$  or  $[\frac{1}{\sqrt{3}} \frac{1}{\sqrt{3}} \frac{1}{\sqrt{3}}]$  as the precoder, and  $P_2$  is the received interference power at PU 2 when SU 1 uses our BBF precoder. *ii) Rx-side IC capability at SU 2:* This IC capability is from SU 2's BIC. It is defined as  $\beta_{rx} = |\text{EVM}| - \max\{\text{SIR}_m\}$ , where  $\text{SIR}_m$  is the signal to interference ratio (SIR) on SU 2's  $m$ th antenna and EVM will be defined in the following. *iii) Error vector magnitude (EVM) of the decoded signals at SU 2:* It is defined as follows:

$$\text{EVM} = 10 \log_{10} \left( \frac{\mathbb{E}[|\hat{X}_s^{[2]}(l, k) - X_s^{[2]}(l, k)|^2]}{\mathbb{E}[|X_s^{[2]}(l, k)|^2]} \right). \quad (19)$$

*iv) Throughput of secondary and primary networks:* The throughput of the primary and secondary networks are extrapolated based on the measured EVM at SU 2 and PU 2, respectively. To calculate throughput, we use

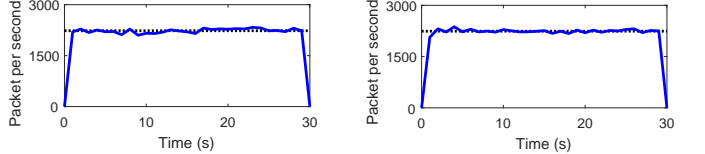
$$r = \frac{N_{sc}}{N_{fft} + N_{cp}} \cdot b \cdot \eta_t \cdot \gamma(\text{EVM}), \quad (20)$$

where  $N_{sc}$ ,  $N_{fft}$ , and  $N_{cp}$  denote number of used subcarriers, FFT points, and the length of cyclic prefix, respectively.  $b$  is the sampling rate in MSps.  $\eta_t$  is the portion of available airtime being used for signal transmissions.  $\gamma(\text{EVM})$  is the average number of bits carried by one subcarrier. This parameter is specified in Table II and Table III for WiFi-like PHY and LTE-like PHY, respectively.

### C. Coexistence with Commercial Wi-Fi Devices

We first consider primary network 1 in Table I. The two WiFi devices (Alfa 802.11n dongles with Atheros Chipset) in this primary network are connected in the ad-hoc mode, and they send data packets to each other as shown in Fig. 3. These two devices are placed at the spots marked by blue squares in Fig. 9. The secondary network is also specified in Table I. Each secondary device is equipped with two antennas. We place the two secondary devices at location 1 in Fig. 9.

**Primary Network:** We first study the performance of the primary devices with and without spectrum sharing. Fig. 10(a) shows the measured packet delivery rate between the two primary devices in the absence of secondary devices (i.e., the secondary devices are turned off). Fig. 10(b) shows the measured result when the secondary devices conduct their transmissions in Phase II (see Fig. 8(b)). It can be seen that,



(a) Packet delivery rate in interference-free scenario.  
(b) Packet delivery rate in spectrum sharing scenario.

Fig. 10: Packet delivery rate of the primary network in interference-free and spectrum sharing scenarios.

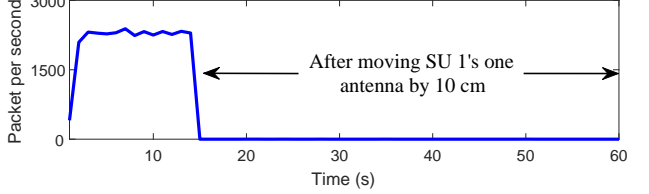
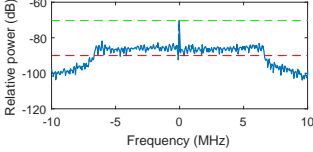


Fig. 11: Packet delivery rate of the primary network before and after moving SU 1's one antenna by 10 cm.

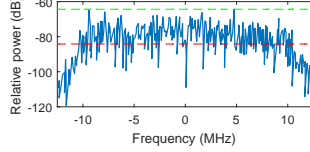
in both cases, the primary network achieves almost the same packet delivery rate. This indicates that the primary network is almost not affected by the secondary network.

How is the interference from the secondary transmitter handled? Is it because of the BBF on the secondary transmitter? To answer these questions, we conduct another experiment. When both primary and secondary networks are transmitting, we move one of the secondary transmitter's antennas about 10 cm. Fig. 11 shows the packet delivery rate of the primary network before and after the antenna movement. We can see that the movement of SU 1's one antenna results in a steep drop of primary network's packet delivery rate. This indicates that it is SU 1's BBF that mitigates the interference for PU 2.

**Secondary Network:** We now shift our focus to the secondary network. We first check the strength of signal and interference at the secondary receiver. Fig. 12 shows the measured results on one of SU 2's antennas. We can see that the signal and interference at the secondary receiver are at the similar level. This observation also holds for the another antenna. We then check the performance of the secondary receiver in the presence of interference from the primary transmitter. To do so, we conduct three experiments: i) interference-free transmission of the secondary network (secondary devices only, no primary devices); ii) spectrum-sharing transmission with SU 2 using our proposed BIC; and iii) spectrum-sharing transmission with SU 2 using ZF signal detection. The measured results are presented in Fig. 13. It is clear to see that, with the aid of BIC, the secondary receiver can successfully decode its desired signals. Compared to the interference-free scenario, the EVM degradation is about 3.8 dB. The conventional ZF signal detection method cannot decode the signal in the presence of interference. This shows the effectiveness of our proposed BIC technique. A demo video of our real-time spectrum sharing scheme can be found in [12].

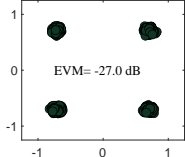


(a) Received interference from PU 1 at SU 2's first antenna.

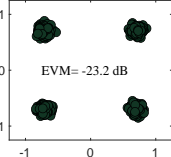


(b) Received signal from SU 1 at SU 2's first antenna.

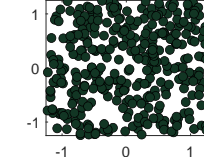
Fig. 12: Relative power spectral density of the received signal and interference at the secondary receiver's first antenna.



(a) Interference-free scenario.



(b) BIC for spectrum sharing scenario.



(c) ZF for spectrum sharing scenario.

Fig. 13: Constellation diagram of the decoded signals at the secondary receiver (SU 2) in three different experiments.

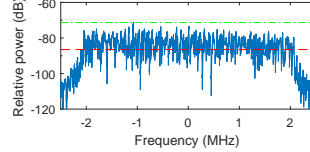
#### D. Network Setting: ( $M_p = 1, M_s = 2$ )

We now consider the CRN in Fig. 8 when the primary devices have one antenna ( $M_p = 1$ ) and the secondary devices have two antennas ( $M_s = 2$ ). Primary networks 2 and 3 specified in Table I are used in our experiments.

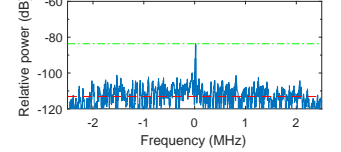
*1) A Case Study:* As a case study, we use primary network 3 (CDMA-like) in Table I and place the secondary devices at location 1 to examine the proposed spectrum sharing scheme.

**Tx-Side IC Capability:** We first want to quantify the tx-side IC capability at the secondary transmitter (SU 1) from its BBF. To do so, we conduct the following experiments. We turn off the primary transmitter (PU 1) and measure the received interference at the primary receiver (PU 2) in two cases: (i) using  $\left[\frac{1}{\sqrt{2}} \quad \frac{1}{\sqrt{2}}\right]$  as the precoder; and (ii) using our proposed beamforming precoder in (7) and (8) with  $\alpha_1 = 1$ . Fig. 14 presents our experimental results. We can see that, in the first case, the relative power spectral density of PU 2's received interference is about  $-87$  dB. In the second case, the relative power spectral density of PU 2's received interference is about  $-113$  dB. Comparing these two cases, we can see that the tx-side IC capability from BBF is about  $113 - 87 = 26$  dB. We note that, based on our observations, the relative power spectral density of the noise at PU 2 is in the range of  $-120$  dB to  $-110$  dB. Therefore, thanks to BBF, the interference from the secondary transmitter to the primary receiver is at the noise level.

**Rx-Side IC Capability, EVM, and Data Rate:** We now study the performance of the secondary receiver (SU 2). First, we measure SIR at SU 2. Fig. 15 shows our measured results on SU 2's first antenna. We can see that the relative power spectral density of its received signal and interference is  $-83$  dB and  $-73$  dB, respectively. This indicates that the SIR on SU 2's first antenna is  $-10$  dB (assuming that noise is negligible). Using the same method, we measured that the SIR on SU 2's second antenna is  $-12$  dB.

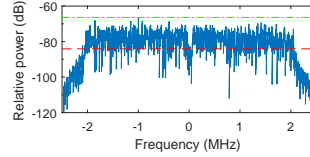


(a) SU 1 uses  $\left[\frac{1}{\sqrt{2}} \quad \frac{1}{\sqrt{2}}\right]$  as the precoder.

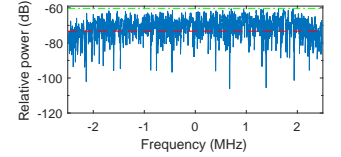


(b) SU 1 uses our BBF technique.

Fig. 14: Relative power spectral density of PU 2's received interference from two-antenna SU 1 in two cases.



(a) SU 2's received signal on its first antenna.

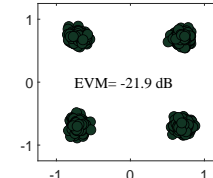


(b) SU 2's received interference on its first antenna.

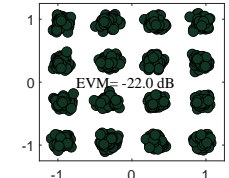
Fig. 15: Relative power spectral density of SU 2's received signal and interference on its first antenna.

We measure the EVM of SU 2's decoded signals in the presence of interference. Fig. 16(a–b) present the constellation of the decoded signals at SU 2. It is evident that SU 2 can decode both QPSK and 16QAM signals from SU 1 in the presence of interference from PU 1. The EVM is  $-21.9$  dB when QPSK is used for the secondary network and  $-22$  dB when 16QAM is used for the secondary network. As a benchmark, Fig. 16(c–d) present the experimental results when there is no interference from PU 1. Comparing Fig. 16(a–b) with Fig. 16(c–d), we can see that SU 2 can effectively cancel the interference from PU 1.

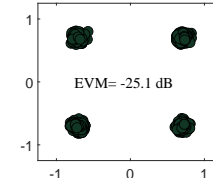
Finally, we calculate SU 2's IC capability and throughput. Based on the SIR on SU 2's antennas and the EVM of its decoded signals, SU 2's IC capability is  $10 + 21.9 = 31.9$  dB in this case. Based on (20) and the measured EVM, the throughput (data rate) of secondary network is extrapolated to be 4.5 Mbps.



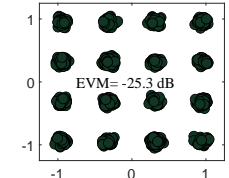
(a) Decoded QPSK signals in spectrum sharing scenario.



(b) Decoded 16QAM signals in spectrum sharing scenario.

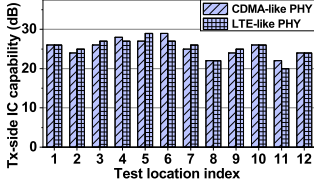


(c) Decoded QPSK signals in interference-free scenario.

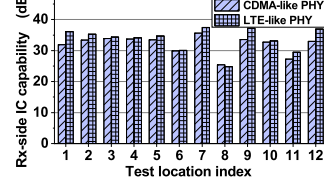


(d) Decoded 16QAM signals in interference-free scenario.

Fig. 16: Constellation diagram of decoded signals at SU 2: our spectrum sharing scheme versus interference-free scenario.

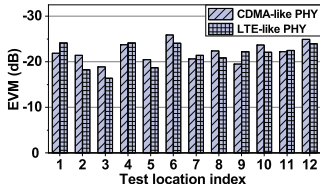


(a) Tx-side IC capability from the secondary transmitter's BBF.

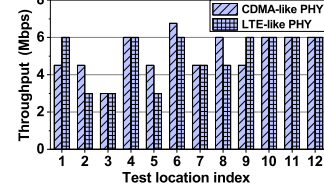


(b) Rx-side IC capability from the secondary receiver's BIC.

Fig. 17: Tx-side and rx-side IC capabilities of the secondary network for ( $M_p = 1, M_s = 2$ ) setting.



(a) EVM of the decoded signals at the secondary receiver.



(b) Throughput of the secondary network.

Fig. 18: Performance of the secondary network in the proposed spectrum sharing scheme for ( $M_p = 1, M_s = 2$ ) setting.

2) *Experimental Results at all Locations:* We now extend our experiments from one location to all the 12 locations and present the measured results as follows.

**Tx-Side IC Capability:** Fig. 17(a) presents the tx-side IC capability of the two-antenna secondary transmitter (SU 1). We can see that the secondary transmitter achieves a minimum of 20.0 dB and an average of 25.3 dB IC capability across all the 12 locations.

**Rx-Side IC Capability:** Fig. 17(b) presents the rx-side IC capability of the two-antenna secondary receiver. We can see that the secondary receiver achieves a minimum of 25.0 dB, a maximum of 38.0 dB, and an average of 32.8 dB IC capability across all the 12 locations, regardless of the PHY used for the primary network.

**Rx-Side EVM:** Fig. 18(a) presents the EVM of the decoded signals at the two-antenna secondary receiver in the presence of interference from the primary transmitter. We can see that in all the locations, although the EVM varies, the EVM achieves an average of  $-21.8$  dB, regardless of the PHY used for the primary network.

**Throughput of Secondary Network:** Based on the measured EVM at the secondary receiver, we extrapolate the achievable data rate in the secondary network using (20). Fig. 18(b) presents the results. As we can see, the secondary network achieves a minimum of 3.0 Mbps data rate, a maximum of 6.7 Mbps, and an average of 5.1 Mbps across all the 12 locations. Note that this data rate is achieved by the secondary network in 5 MHz bandwidth, and the secondary transmitter's power is controlled so that its interference at the primary receiver (after BBF) remains at the noise level.

3) *BBF versus Other Beamforming Techniques:* As BBF is the core component of our spectrum sharing scheme, we would like to further examine its performance by comparing it against the following two beamforming techniques.

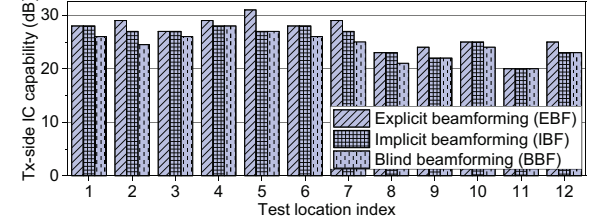


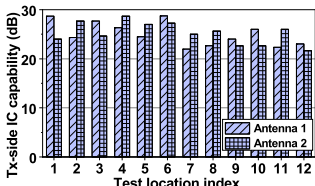
Fig. 19: Tx-side IC capability of the three beamforming techniques when the secondary device has three antennas.

- *Explicit Beamforming (EBF):* In this technique, the secondary transmitter (SU 1) has knowledge of *forward* channel between itself and the primary receiver (PU 2), i.e.,  $\mathbf{H}_{sp}^{[1]}(k)$ . The forward channel knowledge is obtained through explicit channel feedback. Specifically, SU 1 sends a null data packet (NDP) to PU 2, which estimates the channel and feed the estimated channel information back to SU 1. After obtaining the forward channel  $\mathbf{H}_{sp}^{[1]}(k)$ , SU 1 constructs the precoder by  $\mathbf{P}(k) = \text{mineigvectors}(\mathbf{H}_{sp}^{[1]}(k))$ , where  $k$  is subcarrier index.
- *Implicit Beamforming (IBF):* In this technique, the secondary transmitter (SU 1) has knowledge of *backward* channel from the primary receiver (PU 2) to itself, i.e.,  $\mathbf{H}_{ps}^{[1]}(k)$ . The backward channel knowledge is obtained through implicit channel feedback. Specifically, PU 2 sends a null data packet (NDP) to SU 1. SU 1 first estimates the backward channel  $\mathbf{H}_{ps}^{[1]}(k)$ . It then constructs the precoder by  $\mathbf{P}(k) = \text{mineigvectors}(\mathbf{H}_{ps}^{[1]}(k))$ , where  $k$  is subcarrier index. Channel calibration has been performed at SU 1 before signal transmission.

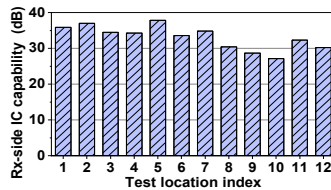
We conduct experiments to measure the tx-side IC capability of these three beamforming techniques. Fig. 19 depicts our results. We can see that, compared to EBF, our proposed BBF has a maximum of 4.5 dB and an average of 2.1 dB degradation. Compared to IBF, our proposed BBF has a maximum of 2.5 dB and an average of 1.0 dB degradation. The results show that the proposed BBF has competitive performance compared to EBF and IBF. We note that, although offering better performance, EBF and IBF cannot be used in underlay CRNs as they require knowledge and cooperation from the primary devices.

#### E. Network Setting: ( $M_p = 2, M_s = 3$ )

We now study the CRN in Fig. 8 when the primary devices have two antennas and the secondary devices have three antennas (i.e.,  $M_p = 2$  and  $M_s = 3$ ). The primary devices use their two antennas for spatial multiplexing. That is, two independent data streams are transferred in the primary network. The secondary devices use their spatial DoF provided by their three antennas for both interference management and signal transmission. Indeed, one data stream is transferred in the secondary network. The primary network uses LTE-like PHY (see primary network 2 in Table I) for data transmission. We study our spectrum sharing scheme in this CRN and report the measured results below.

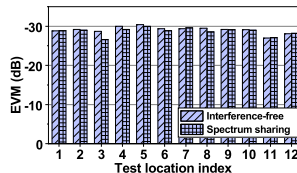


(a) Tx-side IC capability from the secondary transmitter's BBF.

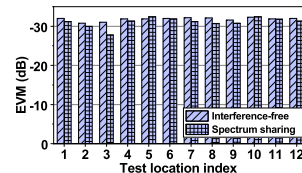


(b) Rx-side IC capability from the secondary receiver's BIC.

Fig. 20: Tx-side and rx-side IC capabilities of the secondary network for ( $M_p=2, M_s=3$ ) setting.



(a) EVM of the decoded data stream 1 at the primary receiver.



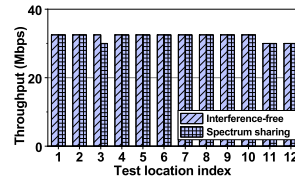
(b) EVM of the decoded data stream 2 at the primary receiver.

Fig. 21: EVM of the two data streams in the primary network with and without the secondary network for ( $M_p=2, M_s=3$ ) setting.

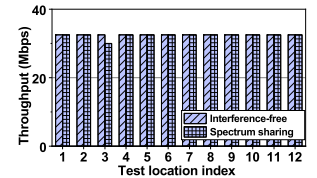
**Tx-Side IC Capability:** In this CRN, since the primary receiver has two antennas, the secondary transmitter needs to cancel its generated interference for both antennas on the primary receiver. We measure the IC capability of our proposed BBF for the primary receiver's both antennas. Fig 20(a) exhibits our measured results. We can see that a three-antenna secondary transmitter can effectively cancel the interference on the primary receiver's both antennas. Specifically, the BBF on the secondary transmitter achieves a minimum of 21.7 dB, a maximum of 28.7 dB, and an average of 25.1 dB IC capability for the primary receiver's two antennas.

**Rx-Side IC Capability:** In this CRN, since the primary transmitter sends two independent data streams, the secondary receiver needs to decode its desired signals in the presence of two interference sources. We measure the rx-side IC capability of our proposed BIC at the three-antenna secondary receiver. Fig 20(b) exhibits our measured results. We can see that the proposed BIC on the secondary receiver achieves a minimum of 26.5 dB, a maximum of 38.1 dB, and an average of 33.0 dB IC capability over the 12 locations. This shows the effectiveness of the proposed BIC in handling unknown interference.

**EVM at Primary Receiver:** We now study the performance of the two data streams in the primary network. We want to see if the presence of secondary network harmfully affects the traffic in the primary network. To do so, we measure the EVM of the decoded two data streams at the primary receiver in two cases: i) in the presence of the secondary network, and ii) in the absence of the secondary network. Fig. 21 presents our measured results. It can be seen that the presence of the secondary network does not visibly affect the EVM performance of the primary network. This indicates that the BBF at the secondary network successfully mitigates the interference from the secondary transmitter to the primary

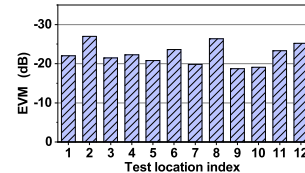


(a) Extrapolated throughput of decoded primary data stream 1.

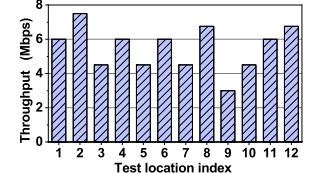


(b) Extrapolated throughput of decoded primary data stream 2.

Fig. 22: Throughput of the two data streams in the primary network with and without the secondary network for ( $M_p=2, M_s=3$ ) setting.



(a) EVM of decoded signals at the secondary receiver.



(b) Throughput of the secondary network.

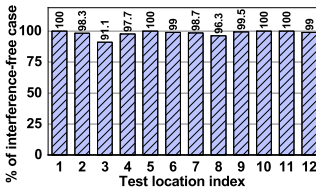
Fig. 23: Performance of the secondary network in the proposed spectrum sharing scheme for ( $M_p=2, M_s=3$ ) setting.

receiver.

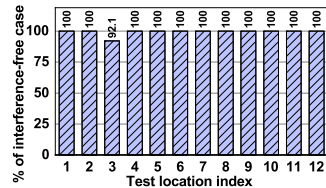
**Throughput of Primary Network:** Based on the measured EVM at the primary receiver, we extrapolate the achievable data rate on each data stream of the primary network using (20). The extrapolated throughput is presented in Fig. 22. Referring to Fig. 22(a), the primary network achieves an average of 32.1 Mbps throughput for its stream 1 in interference-free case and an average of 31.9 Mbps throughput in coexistence with the secondary network. As shown in Fig. 22(b), for its data stream 2, the primary network achieves 32.5 Mbps and 32.3 Mbps throughput on average in the interference-free and spectrum sharing scenarios, respectively. For both data streams, only 0.2 Mbps degradation is observed in the throughput of the primary network.

**EVM at Secondary Receiver:** Having confirmed that the spectrum utilization of secondary network does not degrade the performance of primary network, we now study the achievable performance of the secondary network. Recall that we transfer one data stream in the secondary network. We measure EVM of the decoded signal at the secondary receiver. Fig. 23(a) depicts the measured results. We can see that the EVM at the secondary receiver achieves a minimum of  $-27.7$  dB, a maximum of  $-18.2$  dB, and an average of  $-22.5$  dB over the 12 locations.

**Throughput of Secondary Network:** Based on the measured EVM at the secondary receiver, we extrapolate the achievable data rate of the secondary network using (20). The extrapolated data rate is presented in Fig. 23(b). We can see that the proposed spectrum sharing scheme achieves a minimum of 3.0 Mbps, a maximum of 7.5 Mbps, and an average of 5.5 Mbps over the 12 locations. Note that this data rate is achieved by the secondary network in 5 MHz and without harmfully affecting the primary network.



(a) Measured EVM of primary data streams.



(b) Extrapolated throughput of primary data streams.

Fig. 24: Performance of the proposed spectrum sharing scheme w.r.t. interference-free case for  $(M_p=2, M_s=3)$  setting.

#### F. Summary of Observations

We now summarize the observations from our experimental results as follows:

- **BBF:** BBF demonstrates its capability of handling cross-network interference in CRNs where the secondary network has no knowledge about the primary network. In  $(M_p=1, M_s=2)$  network setting, BBF achieves an average of 25.3 dB IC capability. In  $(M_p=2, M_s=3)$  network setting, BBF achieves an average of 25.1 dB IC capability.
- **BIC:** BIC also demonstrates its capability of decoding the desired signals in the presence of unknown interference. In  $(M_p=1, M_s=2)$  network setting, it achieves an average of 32.8 dB IC capability. In  $(M_p=2, M_s=3)$  network setting, it achieves an average of 33.0 dB IC capability.
- **Primary Network:** The primary network has very small performance degradation when the secondary network shares the spectrum (compared to the case without secondary network). As shown in Fig. 24(a), the average EVM degradation at the primary receiver is 1.6% over the 12 locations. Also, as shown in Fig. 24(b), the average throughput degradation at the primary receiver is 0.7% over the 12 locations.
- **Secondary Network:** Using BBF at its transmitter and BIC at its receiver, the secondary network intends to establish communications by sharing the spectrum with the primary network. The secondary network achieves 1.0 bits/s/Hz in the CRN with  $(M_p=1, M_s=2)$  network setting and 1.1 bits/s/Hz in the CRN with  $(M_p=2, M_s=3)$  network setting.

### VIII. LIMITATIONS AND DISCUSSIONS

While the proposed scheme demonstrates its potential in real-world networks, there are still some issues that remain open and need to be addressed prior to its real applications.

**Primary Traffic Directions:** In our spectrum sharing scheme, we assume that the primary communications are bidirectional and that the pattern of primary traffic is consistent. Under such assumptions, duration and direction of primary traffic are easy to learn for beamforming filter design. In real systems, the pattern of primary traffic might not be consistent. In such a case, a sophisticated learning algorithm is needed for the secondary devices to differentiate the forward and backward transmissions of the primary network.

**Channel Coherence Time:** In static networks (e.g., indoor Wi-Fi), the devices are stationary or moving at a low speed. Then, the channel coherence time is large enough to cover the entire period of primary forward transmission. But in the dynamic networks with highly mobile devices, the channel coherence time may be smaller than the duration of primary forward transmission. In such a case, the secondary network cannot use the entire airtime of primary forward transmission. Instead, it can only access the spectrum when its beamforming filters remain valid (i.e., within the channel coherence time).

**Extension to Large-Scale Networks:** In this work, we presented a spectrum sharing scheme for a small-size CRN consisting of one PU pair and one SU pair. This spectrum sharing scheme can be extended to a large-scale CRN that comprises multiple PU pairs and multiple SU pairs. This is because in most real-world wireless networks (e.g., Wi-Fi and cellular), only one user pair is active on a frequency band at a time. Therefore, our current design is a fundamental building block for spectrum sharing in a large-scale CRN. Nevertheless, extending our design to a large-scale CRN still faces several challenges. First, a secondary device should be capable of learning the active PU devices over time as well as their transmission direction and duration. For a secondary device, how to accurately obtain this information through a learning procedure is a challenging task. Second, primary devices may not be stationary (e.g., vehicular and unmanned aerial networks). How to design an adaptive and intelligent spectrum sharing MAC protocol for the secondary network is another challenging task. These challenges will be addressed in our future work.

### IX. CONCLUSION

In this paper, we proposed a spectrum sharing scheme for an underlay CRN that comprises two primary users and two secondary users. The proposed scheme allows the secondary users to use the spectrum without affecting the throughput of the primary users. The key components of our scheme are two MIMO-based IC techniques: BBF and BIC. BBF enables the secondary transmitter to pre-cancel its generated interference for the primary receiver. BIC enables the secondary receiver to decode its desired signals in the presence of unknown cross-network interference. Collectively, these two IC techniques make it possible for the secondary users to access the spectrum while remaining transparent to the primary users. We have built a prototype of our spectrum sharing scheme on a wireless testbed. We demonstrated that our prototyped secondary devices can coexist with commercial Wi-Fi devices. Extensive experimental results show that, for a secondary user with two or three antennas, BBF and BIC achieve about 25 dB and 33 dB IC capabilities in real wireless environments, respectively.

### APPENDIX A PROOF OF LEMMA 1

We first consider the signal transmission in Phase I and then consider that in Phase II. In Phase I, if the noise is zero, we

have  $\mathbf{Y}(l, k) = \mathbf{H}_{\text{sp}}^{[1]}(k)\mathbf{X}_{\text{p}}^{[1]}(l, k)$ . Then, we have

$$\begin{aligned} \sum_{l=1}^{L_{\text{p}}} \mathbf{Y}(l, k)\mathbf{Y}(l, k)^* &\stackrel{(a)}{=} L_{\text{p}}\mathbb{E}[\mathbf{Y}(l, k)\mathbf{Y}(l, k)^*] \\ &\stackrel{(b)}{=} L_{\text{p}}\mathbf{H}_{\text{sp}}^{[1]}(k)\mathbf{R}_{\text{x}}(k)\mathbf{H}_{\text{sp}}^{[1]}(k)^*, \end{aligned} \quad (21)$$

where (a) follows from that  $\mathbf{Y}(l, k)$  is a stationary random process, which is true in practice; and (b) follows from the definition of  $\mathbf{R}_{\text{x}}(k) = \mathbb{E}[\mathbf{X}_{\text{p}}^{[1]}(l, k)\mathbf{X}_{\text{p}}^{[1]}(l, k)^*]$ .

Based on (21), we have

$$\begin{aligned} \text{Rank}\left(\sum_{l=1}^{L_{\text{p}}} \mathbf{Y}(l, k)\mathbf{Y}(l, k)^*\right) &= \text{Rank}\left(L_{\text{p}}\mathbf{H}_{\text{sp}}^{[1]}(k)\mathbf{R}_{\text{x}}(k)\mathbf{H}_{\text{sp}}^{[1]}(k)^*\right) \\ &\leq \text{Rank}(\mathbf{R}_{\text{x}}(k)) \leq M_{\text{p}}. \end{aligned} \quad (22)$$

Inequation (22) indicates that  $\sum_{l=1}^{L_{\text{p}}} \mathbf{Y}(l, k)\mathbf{Y}(l, k)^*$  has at least  $M_{\text{s}} - M_{\text{p}}$  eigenvectors that correspond to zero eigenvalues. This further indicates that  $[\mathbf{U}_1, \mathbf{U}_2, \dots, \mathbf{U}_{M_{\text{e}}}]$  in (7) are corresponding to zero eigenvalues. Therefore, we have

$$\left(\sum_{l=1}^{L_{\text{p}}} \mathbf{Y}(l, k)\mathbf{Y}(l, k)^*\right)\mathbf{U}_m = \mathbf{0}, \quad \text{for } 1 \leq m \leq M_{\text{e}}. \quad (23)$$

Based on (21) and (23), we have

$$\left(L_{\text{p}}\mathbf{H}_{\text{sp}}^{[1]}(k)\mathbf{R}_{\text{x}}(k)\mathbf{H}_{\text{sp}}^{[1]}(k)^*\right)\mathbf{U}_m = \mathbf{0}, \quad \text{for } 1 \leq m \leq M_{\text{e}}. \quad (24)$$

In real wireless environments, we have  $\text{Rank}(\mathbf{H}_{\text{sp}}^{[1]}(k)) = M_{\text{p}}$  and  $\text{Rank}(\mathbf{R}_{\text{x}}(k)) = M_{\text{p}}$ . Therefore, the following equation can be deducted from (24).

$$\mathbf{H}_{\text{sp}}^{[1]}(k)^*\mathbf{U}_m = \mathbf{0}, \quad \text{for } 1 \leq m \leq M_{\text{e}}. \quad (25)$$

Based on (8) and (25), we have

$$\mathbf{H}_{\text{sp}}^{[1]}(k)^*\mathbf{P}(k) = \sum_{m=1}^{M_{\text{e}}} \alpha_m \mathbf{H}_{\text{sp}}^{[1]}(k)^*\mathbf{U}_m = \mathbf{0}. \quad (26)$$

We now consider signal transmission in Phase II (see Fig. 4(b)). Denote  $\mathbf{H}_{\text{ps}}^{[2]}$  as the matrix representation of the channel from SU 1 to PU 2 on subcarrier  $k$  in Phase II. Given that the forward and backward channels in the two phases are reciprocal, we have  $\mathbf{H}_{\text{ps}}^{[2]} = (\mathbf{H}_{\text{sp}}^{[1]})^T$ . Then, we have

$$\mathbf{H}_{\text{ps}}^{[2]}(k)\overline{\mathbf{P}(k)} = (\mathbf{H}_{\text{sp}}^{[1]})^T\overline{\mathbf{P}(k)} = \overline{\mathbf{H}_{\text{sp}}^{[1]}(k)^*\mathbf{P}(k)} = \mathbf{0}. \quad (27)$$

It means that the precoding vector  $\overline{\mathbf{P}(k)}$  is orthogonal to the interference channel  $\mathbf{H}_{\text{ps}}^{[2]}(k)$ . Therefore, we conclude that the proposed beamforming scheme can completely pre-cancel the interference from the secondary transmitter at the primary receiver in Phase II.

## APPENDIX B PROOF OF LEMMA 2

For notational simplicity, we denote  $\mathbf{H}(k)$  as the compound channel between the SU 2 and the two transmitters (SU 1 and PU 1), i.e.,  $\mathbf{H}(k) = [\mathbf{H}_{\text{ss}}^{[2]}(k)\mathbf{P}(k) \quad \mathbf{H}_{\text{sp}}^{[2]}(k)]$ ; we also denote  $\mathbf{X}(l, k)$  as the compound transmit signals at the two

transmitters, i.e.,  $\mathbf{X}(l, k) = [X_{\text{s}}^{[2]}(l, k) \quad \mathbf{X}_{\text{p}}^{[2]}(l, k)]^T$ . Then, in noise-negligible scenarios, (9) can be rewritten as:

$$\mathbf{Y}(l, k) = \mathbf{H}(k)\mathbf{X}(l, k). \quad (28)$$

By defining  $\mathbf{R}_{\text{x}}$  as the autocorrelation matrix of the compound transmit signals, we have

$$\mathbf{R}_{\text{x}} = \mathbb{E}(\mathbf{XX}^H) \stackrel{(a)}{=} \begin{bmatrix} R_{\text{xs}} & \mathbf{0} \\ \mathbf{0} & \mathbf{R}_{\text{xp}} \end{bmatrix} = \begin{bmatrix} 1 & \mathbf{0} \\ \mathbf{0} & \mathbf{R}_{\text{xp}} \end{bmatrix}, \quad (29)$$

where  $R_{\text{xs}}$  is the autocorrelation of SU 1's transmit signal and  $\mathbf{R}_{\text{xp}}$  is the autocorrelation matrix of PU 1's transmit signals. (a) follows from our assumption that the transmit signal from SU 1 is independent of the transmit signals from PU 1. Note that  $\mathbf{R}_{\text{xp}}$  is not necessarily an identity matrix since the signals from PU 1's different antennas might be correlated.

Based on (18), (28), and (29), we have

$$\begin{aligned} \mathbf{G}(k) &= \left[ \sum_{(l, k') \in \mathcal{Q}_k} \mathbf{Y}(l, k')\mathbf{Y}(l, k')^H \right]^+ \left[ \sum_{(l, k') \in \mathcal{Q}_k} \mathbf{Y}(l, k')X_s^{[2]}(l, k')^* \right] \\ &\stackrel{(a)}{=} \mathbb{E}[\mathbf{Y}(l, k)\mathbf{Y}(l, k)^*]^+ \mathbb{E}[\mathbf{Y}(l, k)X_s^{[2]}(l, k)^*] \\ &\stackrel{(b)}{=} [\mathbf{H}(k)\mathbf{R}_{\text{x}}\mathbf{H}(k)^*]^+ [\mathbf{H}(k)\mathbf{I}_1], \end{aligned} \quad (30)$$

where (a) follows from our assumption that the amount of reference signals is sufficient to achieve convergence of  $\mathbf{G}(k)$ ; (b) follows from the definition that  $\mathbf{I}_1$  is a vector where its first entry is 1 and all other entries are 0.

Based on (10) and (30), we have

$$\begin{aligned} \hat{X}_s^{[2]}(l, k) &= \mathbf{G}(k)^*\mathbf{Y}(l, k) \\ &= \left\{ [\mathbf{H}(k)\mathbf{R}_{\text{x}}\mathbf{H}(k)^*]^+ [\mathbf{H}(k)\mathbf{I}_1] \right\}^* \mathbf{H}(k)\mathbf{X}(l, k) \\ &= X_s^{[2]}(l, k), \quad \forall l, k. \end{aligned} \quad (31)$$

## REFERENCES

- [1] P. Kheirkhah Sangdeh, H. Pirayesh, H. Zeng, and H. Li, "A practical underlay spectrum sharing scheme for cognitive radio networks," in *IEEE International Conference on Computer Communications (INFOCOM)*, pp. 2521–2529, 2019.
- [2] A. Goldsmith, S. A. Jafar, I. Maric, and S. Srinivasa, "Breaking spectrum gridlock with cognitive radios: An information theoretic perspective," *Proceedings of the IEEE*, vol. 97, no. 5, pp. 894–914, 2009.
- [3] R. Sarvendranath and N. B. Mehta, "Exploiting power adaptation with transmit antenna selection for interference-outage constrained underlay spectrum sharing," *IEEE Transactions on Communications*, vol. 68, no. 1, pp. 480–492, 2020.
- [4] B. Venkatesh, N. B. S. Krishna, and S. Chouhan, "Distributed optimal power allocation using game theory in underlay cognitive radios," in *Data Communication and Networks*, pp. 295–304, 2020.
- [5] R. M. Rao, H. S. Dhillon, V. Marojevic, and J. H. Reed, "Analysis of worst-case interference in underlay radar-massive MIMO spectrum sharing scenarios," in *Proc. of IEEE Global Communications Conference (GLOBECOM)*, 2019.
- [6] P. Lan, C. Zhai, L. Chen, B. Gao, and F. Sun, "Optimal power allocation for bi-directional full duplex underlay cognitive radio networks," *IET Communications*, vol. 12, no. 2, pp. 220–227, 2017.
- [7] Y. Wang, P. Ren, Q. Du, and L. Sun, "Optimal power allocation for underlay-based cognitive radio networks with primary user's statistical delay QoS provisioning," *IEEE Transactions on Wireless Communications*, vol. 14, no. 12, pp. 6896–6910, 2015.
- [8] Y. Liu, Z. Ding, M. Elkashlan, and J. Yuan, "Non-orthogonal multiple access in large-scale underlay cognitive radio networks," *IEEE Transactions on Vehicular Technology*, vol. 65, no. 12, pp. 10152–10157, 2016.

- [9] S. Dadallage, C. Yi, and J. Cai, "Joint beamforming, power, and channel allocation in multiuser and multichannel underlay MISO cognitive radio networks," *IEEE Transactions on Vehicular Technology*, vol. 65, no. 5, pp. 3349–3359, 2016.
- [10] V.-D. Nguyen, L.-N. Tran, T. Q. Duong, O.-S. Shin, and R. Farrell, "An efficient precoder design for multiuser MIMO cognitive radio networks with interference constraints," *IEEE Transactions on Vehicular Technology*, vol. 66, no. 5, pp. 3991–4004, 2017.
- [11] S. Kusaladharma and C. Tellambura, "Secondary user interference characterization for spatially random underlay networks with massive MIMO and power control," *IEEE Transactions on Vehicular Technology*, vol. 66, no. 9, pp. 7897–7912, 2017.
- [12] P. Kheirkhah Sangdeh, A. Quadri, and H. Zeng, "Demo: A practical spectrum sharing solution." [http://www.ece.louisville.edu/hzeng/spectrum\\_sharing.html](http://www.ece.louisville.edu/hzeng/spectrum_sharing.html), 2019. Online; accessed 13 April 2019.
- [13] W. D. Horne, "Adaptive spectrum access: Using the full spectrum space," in *Proceedings of Telecommunications Policy Research Conference (TPRC)*, 2003.
- [14] H. Pennanen, A. Tölli, and M. Latva-aho, "Multi-cell beamforming with decentralized coordination in cognitive and cellular networks," *IEEE Transactions on Signal Processing*, vol. 62, no. 2, pp. 295–308, 2014.
- [15] E. A. Gharavol, Y.-C. Liang, and K. Mouthaan, "Robust downlink beamforming in multiuser MISO cognitive radio networks with imperfect channel-state information," *IEEE Transactions on Vehicular Technology*, vol. 59, no. 6, pp. 2852–2860, 2010.
- [16] W. Xu, Y. Cui, H. Zhang, G. Y. Li, and X. You, "Robust beamforming with partial channel state information for energy efficient networks," *IEEE Journal on Selected Areas in Communications*, vol. 33, no. 12, pp. 2920–2935, 2015.
- [17] Y. Huang, Q. Li, W.-K. Ma, and S. Zhang, "Robust multicast beamforming for spectrum sharing-based cognitive radios," *IEEE Transactions on Signal Processing*, vol. 60, no. 1, p. 527, 2012.
- [18] A. Alabbasi, Z. Rezki, and B. Shihada, "Energy efficiency and SINR maximization beamformers for spectrum sharing with sensing information," *IEEE Transactions on Wireless Communications*, vol. 13, no. 9, pp. 5095–5106, 2014.
- [19] M. C. Filippou, P. De Kerret, D. Gesbert, T. Ratnarajah, A. Pastore, and G. A. Ropokis, "Coordinated shared spectrum precoding with distributed CSIT," *IEEE Transactions on Wireless Communications*, vol. 15, no. 8, pp. 5182–5192, 2016.
- [20] S. He, Y. Huang, H. Wang, S. Jin, and L. Yang, "Leakage-aware energy-efficient beamforming for heterogeneous multicell multiuser systems," *IEEE Journal on Selected Areas in Communications*, vol. 32, no. 6, pp. 1268–1281, 2014.
- [21] Y. Y. He and S. Dey, "Sum rate maximization for cognitive MISO broadcast channels: Beamforming design and large systems analysis," *IEEE Transactions on Wireless Communications*, vol. 13, no. 5, pp. 2383–2401, 2014.
- [22] A. Afana, V. Asghari, A. Ghayeb, and S. Affes, "On the performance of cooperative relaying spectrum-sharing systems with collaborative distributed beamforming," *IEEE Transactions on Communications*, vol. 62, no. 3, pp. 857–871, 2014.
- [23] A. Afana, T. M. Ngatche, and O. A. Dobre, "Cooperative AF relaying with beamforming and limited feedback in cognitive radio networks," *IEEE Communications Letters*, vol. 19, no. 3, pp. 491–494, 2015.
- [24] N. Nandan, S. Majhi, and H.-C. Wu, "Maximizing secrecy capacity of underlay MIMO-CRN through bi-directional zero-forcing beamforming," *IEEE Transactions on Wireless Communications*, vol. 17, no. 8, pp. 5327–5337, 2018.
- [25] N. Nandan, S. Majhi, and H.-C. Wu, "Secure beamforming for MIMO-NOMA-based cognitive radio network," *IEEE Communications Letters*, vol. 22, no. 8, pp. 1708–1711, 2018.
- [26] M. Zhang and Y. Liu, "Secure beamforming for untrusted MISO cognitive radio networks," *IEEE Transactions on Wireless Communications*, vol. 17, no. 7, pp. 4861–4872, 2018.
- [27] R. Zhang, F. Gao, and Y.-C. Liang, "Cognitive beamforming made practical: Effective interference channel and learning-throughput tradeoff," *IEEE Transactions on Communications*, vol. 2, no. 58, pp. 706–718, 2010.
- [28] Z. Chen, C.-X. Wang, X. Hong, J. Thompson, S. A. Vorobyov, F. Zhao, and X. Ge, "Interference mitigation for cognitive radio MIMO systems based on practical precoding," *Physical communication*, vol. 9, pp. 308–315, 2013.
- [29] M. H. Al-Ali and K. Ho, "Transmit precoding in underlay MIMO cognitive radio with unavailable or imperfect knowledge of primary interference channel," *IEEE Transactions on Wireless Communications*, vol. 15, no. 8, pp. 5143–5155, 2016.
- [30] S.-M. Cai and Y. Gong, "Cognitive beamforming for throughput maximization with statistical cross channel state information," *IEEE Communications Letters*, vol. 18, no. 11, pp. 2031–2034, 2014.
- [31] Y. Noam and A. J. Goldsmith, "Blind null-space learning for MIMO underlay cognitive radio with primary user interference adaptation," *IEEE Transactions on Wireless Communications*, vol. 12, no. 4, pp. 1722–1734, 2013.
- [32] T. Xu, L. Ma, and G. Sternberg, "Practical interference alignment and cancellation for MIMO underlay cognitive radio networks with multiple secondary users," in *Proceedings of IEEE Global Communications Conference (GLOBECOM)*, pp. 1009–1014, 2013.
- [33] O. Rousseaux, G. Leus, and M. Moonen, "A blind multi-user MIMO transceiver using code modulation in a multipath context," in *Proceedings of International Conference on Digital Signal Processing*, vol. 1, pp. 267–270, 2002.
- [34] J. H. Winters, "Signal acquisition and tracking with adaptive arrays in the digital mobile radio system IS-54 with flat fading," *IEEE Transactions on Vehicular Technology*, vol. 42, no. 4, pp. 377–384, 1993.
- [35] S. Gollakota, F. Adib, D. Katabi, and S. Seshan, "Clearing the RF smog: Making 802.11n robust to cross-technology interference," in *Proceedings of ACM SIGCOMM*, vol. 41, pp. 170–181, 2011.
- [36] Q. Yan, H. Zeng, T. Jiang, M. Li, W. Lou, and Y. T. Hou, "Jamming resilient communication using MIMO interference cancellation," *IEEE Transactions on Information Forensics and Security*, vol. 11, no. 7, pp. 1486–1499, 2016.
- [37] W. Shen, P. Ning, X. He, H. Dai, and Y. Liu, "MCR decoding: A MIMO approach for defending against wireless jamming attacks," in *Proceedings of IEEE Conference on Communications and Network Security (CNS)*, pp. 133–138, 2014.
- [38] C. Shepard, H. Yu, N. Anand, E. Li, T. Marzetta, R. Yang, and L. Zhong, "Argos: Practical many-antenna base stations," in *Proceedings of the 18th annual international conference on Mobile computing and networking*, pp. 53–64, 2012.
- [39] IEEE 802.11ac, "IEEE standard for information technology local and metropolitan area networks part 11: Wireless LAN medium access control (MAC) and physical layer (PHY) specifications amendment 5: Enhancements for higher throughput," *IEEE Standards 802.11ac*, 2014.
- [40] M. T. Kawser, N. I. B. Hamid, M. N. Hasan, M. S. Alam, and M. M. Rahman, "Downlink SNR to CQI mapping for different multiple-antenna techniques in LTE," *Int. J. Inf. Electron. Eng.*, vol. 2, no. 5, p. 757, 2012.
- [41] T. ETSI, "136 213 v12. 3.0 technical specification LTE," *Evolved Universal Terrestrial Radio Access (E-UTRA)*.



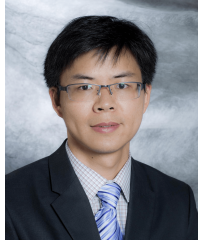
**Pedram Kheirkhah Sangdeh** received his B.Sc. degree in Electrical and Computer Engineering from Iran University of Science and Technology, Tehran, Iran, in 2011, and his M.Sc. degree in Electrical and Computer Engineering from the College of Engineering, University of Tehran, Tehran, Iran, in 2014. He is currently working toward a Ph.D. degree with the Department of Electrical and Computer Engineering at the University of Louisville, Louisville, KY, USA. His research interests include performance analysis and implementation of innovative protocols for the next generation of wireless networks.



**Hossein Pirayesh** received his B.Sc. degree in Electrical Engineering from Karaj Islamic Azad University, Karaj, Iran in 2013 and his M.Sc. degree in Electrical Engineering from Iran University of Science and Technology, Tehran, Iran in 2016. Since 2017, he has been working toward his Ph.D. degree in the Department of Electrical and Computer Engineering at the University of Louisville, Louisville, KY, USA. His current research is focused on wireless communications and networking, including theoretical analysis, algorithm and protocol design, and system implementation.



**Adnan Quadri** received the B.Sc. degree in Electronics & Telecommunication Engineering from the North South University, Dhaka, Bangladesh in 2011, and the M.Sc. degree in Electronics and Electrical Engineering from the University of North Dakota, Grand Forks, ND, USA in 2018. He is currently pursuing the Ph.D. degree with the Department of Electrical and Computer Engineering at the University of Louisville, Louisville, KY, USA. His research interests and experience are in the next generation wireless communication systems and information communication technologies.



**Huacheng Zeng** (SM'20) is an Assistant Professor of Electrical and Computer Engineering at the University of Louisville, Louisville, KY. He holds a Ph.D. degree in Computer Engineering from Virginia Tech, Blacksburg, VA. He worked as Senior System Engineer on communications system design at Marvell Semiconductor, Santa Clara, CA. His research interest is in wireless networking and mobile computing, including algorithm and protocol design, interference management, physical-layer security, and learning-based wireless applications. He is a recipient of the NSF CAREER Award.